ICAS-88-3.11.2

VORTICAL FLOWS AROUND DELTA WINGS IN UNSTEADY MANEUVERS AND GUSTS

Rolf Staufenbiel, Bernd Steckemetz, Shangxiang Zhu
Institute for Aeronautics and Astronautics
Technical University Aachen, FRG

Abstract

This paper presents experimental investigations of two delta wings with aspect ratio of 1 and 2 operating under unsteady conditions at high angles of attack and sideslip. It includes the influence of gusts produced by a gust-generator in front of a wing fixed in a wind-tunnel, and a plunging motion caused by a forced motion of the wing. Observed unsteady effects are related to the time-dependent strength of the leading edge vortices and, in particular, to unsteady breakdown phenomena. Displacement of the breakdown points of the L.E. vortices is quantitatively evaluated from water-tunnel flow visualization showing hysteresis loops and considerable time lags. Also considerable changes in lift and pitching moment in symmetrical flow states and rolling moment under unsymmetrical conditions have been found in wind-tunnel tests. Simulations using these experimental data indicate a strong impact on the flight dynamic characteristics of the delta wing configurations.

I. Nomenclature

AR = aspect ratio
b = wing span [m]
c = root chord length [m]
C_L = lift coefficient
C_l = rolling moment coefficient
C_m = pitching moment coefficient
f = frequency [Hz]
k = reduced frequency, $\pi fc/U_\infty$
m = aircraft mass [kg]
Re = Reynolds number, $U_\infty c/\nu$
s = Laplace operator
S = reference area = projected wing area [m^2]
U_∞ = freestream velocity [m/s]
α = angle of attack [degree]
β = angle of sideslip [degree]
ν = kinematic viscosity [m^2/s]

II. Introduction

High-speed aircraft are often projected as delta wing or delta wing-canard configurations with moderate or low aspect ratio. At low speed conditions and in maneuver flights these configurations have to be operated at high angles of attack and sideslip[1,2]. Investigations of delta wings initially [3-5], and in recent years [6-10] point out the importance of delta wing studies especially in unsteady flow.

The flow on the suction side of delta wings is dominated by two leading-edge vortices, which, at higher angles of attack, undergo a marked change of structure well-known as vortex-bursting or vortex-breakdown (Fig. 1). Changing the angle of attack under this condition leads to a strong local displacement of the vortex breakdown position. This causes considerable changes in the forces and moments on the wing. In asymmetric flow conditions the breakdown points are as well asymmetrically located.

In unsteady flight maneuvers or in gust fields the development of the flow field around delta wings is strongly time dependent. The displacement of the burst points is related to the frequency of disturbances in the angle of attack, and fast changes of wing incidence produce large phase lags between the angle of attack and the flow conditions [11-13]. This behaviour can be expected to modify the flight dynamic characteristics compared to steady or quasi-steady flight conditions, insofar as the

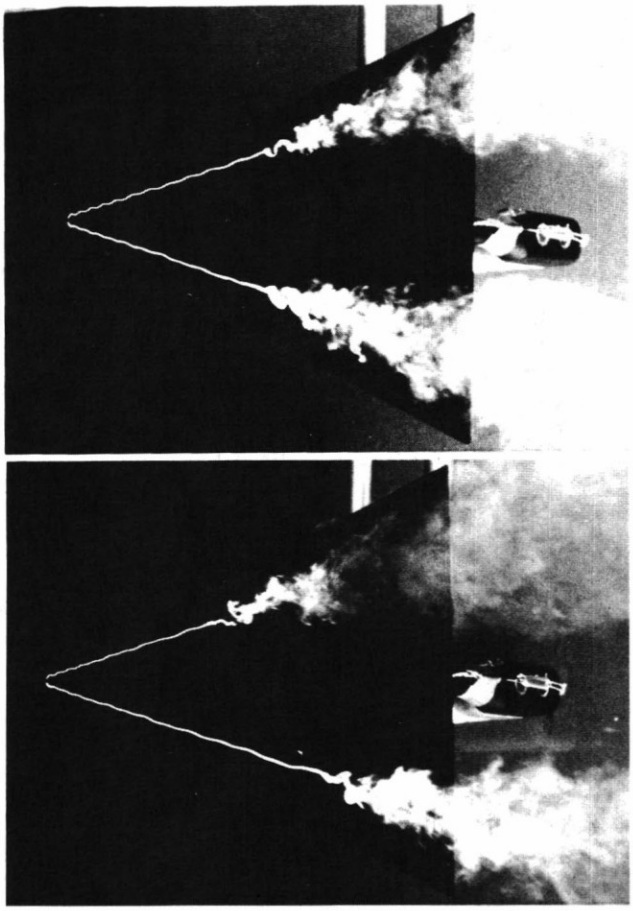

Figure 1. Delta wing of aspect ratio 2 in symmetrical and asymmetrical flow

induced aircraft motion has a feedback effect upon the process of vortex bursting and displacement of the breakdown location.

The present paper deals with the vortex breakdown behaviour in gusts and maneuvers investigated in a water-tunnel and a low speed wind-tunnel. Measurements of forces and moments in the wind-tunnel provide data for a semi-empirical model of the dynamic characteristics. Flow visualization studies in the water-tunnel offer the opportunity to interpret the wind-tunnel results.

III. Test Facilities

The water-tunnel used in the investigations is of the Goettingen type. It has a closed test section with a square cross section of 0.54 m x 0.54 m and a length of 1 m. The flow speed is limited to 4 m/s. For the purpose of visualizing the flow field in three dimensions, the bottom and the walls of the test section are made of glass. The low speed wind-tunnel is also of the Goettingen type with an open test section of 3 m length. The nozzle cross section is 1.5 m in diameter. The fan is driven by a 500 kW motor supplying flow velocities up to 70 m/s.

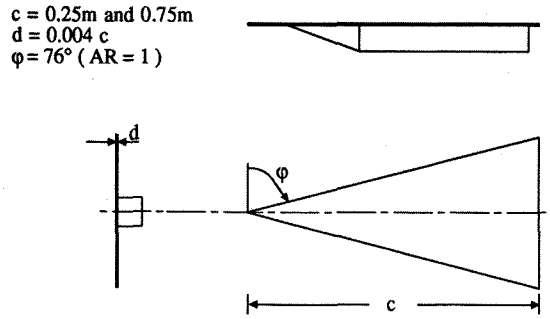

Figure 2. Delta wing configuration of AR=1

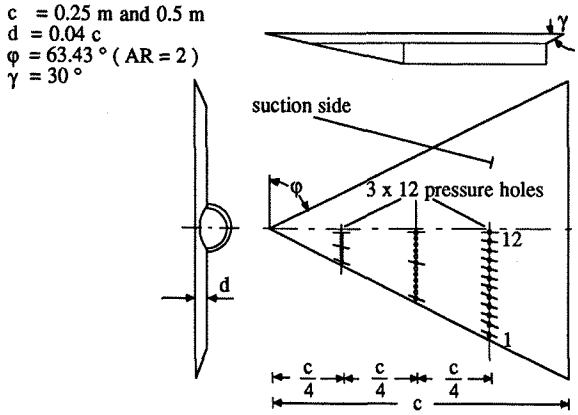

Figure 3. Delta wing configuration of AR=2

Two types of delta wings have been investigated. The first one (Fig. 2) is a wing-body configuration with a thin, flat wing of aspect ratio 1 (AR=1). The chord lengths of the water-tunnel and wind-tunnel models are 0.25 m and 0.75 m, respectively. The second configuration (Fig. 3) is a thicker sharp edged delta wing with an aspect ratio of 2 (AR=2). The root chord lengths of the models used in the water-tunnel and wind-tunnel are 0.25 m and 0.50 m, respectively. This configuration has also been used for pressure measurements. Miniature pressure transducers, connected to the surface by short tubes [14], are installed inside the wing. The tubes are particularly necessary for investigating the wing in plunging motion. The transducers are oriented in such a way that there are no acceleration forces normal to their diaphragms. The force and moment measurements have been done with a wing of composite material to reduce the mass forces on the strain gage balance.

Fig. 4 shows the experimental arrangement. The delta wing is fixed downstream of a gust-generator which is positioned at the exit of the wind-tunnel nozzle. The four vanes of the gust-generator, developed for these investigations, are driven by a 25 kW dc-motor with a r.p.m.-control unit using a crankshaft disk and a connecting rod. Gust frequencies up to 20 Hertz are possible with maximum amplitudes of the vane angle of 10 degrees. Each vane has a spar made of carbon fibre composite.

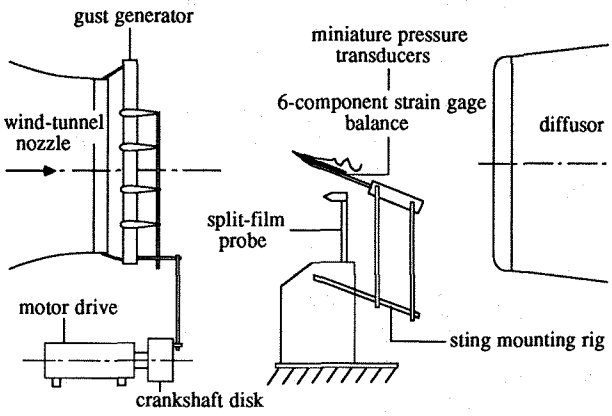

Figure 4. Test facility for the investigation of gusts loads

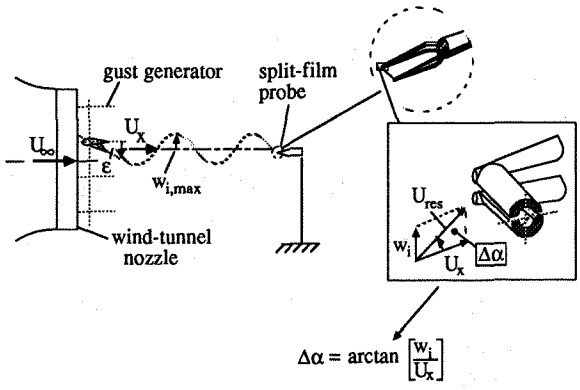

Figure 5. Split-film probe for measurements of gust-induced angles of attack

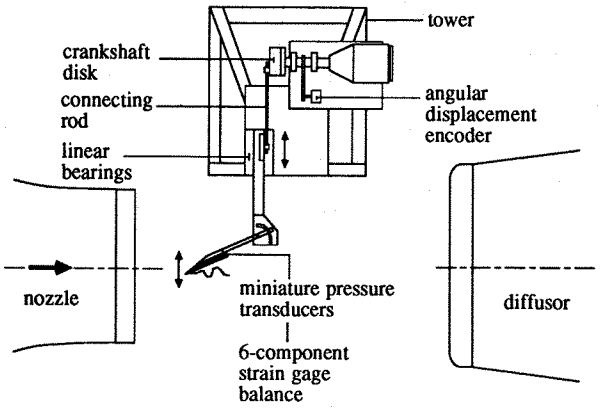

Figure 6. Test assembly for plunging motions (top view)

The vanes have a NACA-0012 profile and otherwise is made of foam coated with a thin skin of light wooden material.

The delta wings are sting-mounted on a 6-component strain gage balance. The balance is fixed to a motorized rig enabling variations of the angles of incidence and sideslip. In a position of half the chord length of the delta wing an adjustable split-film probe is used to measure the unsteady flow velocities. A principal view of this probe, which operates in the CTA mode, is given in Fig. 5. This two-sensor probe provides magnitude and direction of the velocities after a thorough calibration procedure. In this way the probe supplies information about the incremental angle of attack measured at a reference point in the flow field.

The investigations of plunging motions of the delta wings have been done with the assembly pictured in Fig. 6 as viewed from the top. The model is again sting-mounted on the 6-component balance. The sting is fixed to a rig for changing the angles of incidence and sideslip. Driven by a three-phase motor with r.p.m.-control, the plunging motion is performed in a direction normal to gravity vector. In this way model weight and unsteady mass forces produced by the plunging motion act upon different strain gages of the balance, enabling higher plunging amplitudes without saturating the amplifiers. Tests up to 10 Hertz are possible with a maximum incremental angle of attack up to 5 degrees.

Using linear bearings, a crankshaft disk and a connecting rod, it is possible to transpose the rotational motion of the motor drive to a linear harmonic motion of the wing normal to the undisturbed channel flow. Because the harmonic motion of the delta wing is disturbed by the angle of the connecting rod, the connecting rod is more than ten times longer than the maximum amplitude of model motion. The remaining error has been regarded by software means. Information about the angular displacement of the crankshaft disk is given by a sine-potentiometer. Knowledge of this angular displacement together with the rotational frequency enables the incremental angle of attack of the delta wing to be calculated.

The signals of the strain gage balance or the pressure transducers were amplified, converted to digital form and stored by a computer. No hardware filters were used to avoid any loss of information in the collected data. Low-pass-filtering and FFTs have been done afterwards. Test results are obtained as time histories of forces, moments and pressures. Using the time histories, information about amplitudes and phase lags can be extracted.

Only a few modifications had to be done to install the test equipment of Fig. 6 into the water-tunnel. The tests in the water-tunnel used flow visualization techniques and Laser-Doppler-Velocimetry. Water-tunnel investigations were done with a moving model and measurements of gust disturbances were not possible. Hence, comparison between water-tunnel and wind-tunnel results were restricted to maneuvering cases. The flow was made visible using air bubbles, titanium-oxide or milk. A stroboscopic flash lamp was available for triggering purposes. Video pictures were taken with a CCD-video camera and video recorder. A digital image-processing unit was used for quantitative evaluation of the video frames (Fig. 7).

IV. Water-tunnel Results

Steady Flow

The vortex breakdown behaviour of the delta wing with AR=2 is quite different from that with AR=1. Fig. 8 presents the

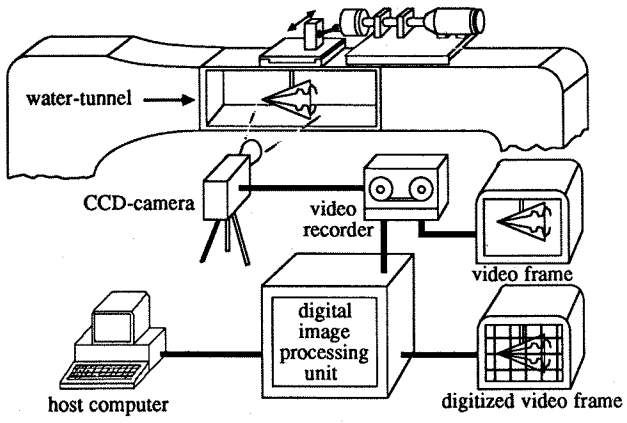

Figure 7. Processing of flow visualization data

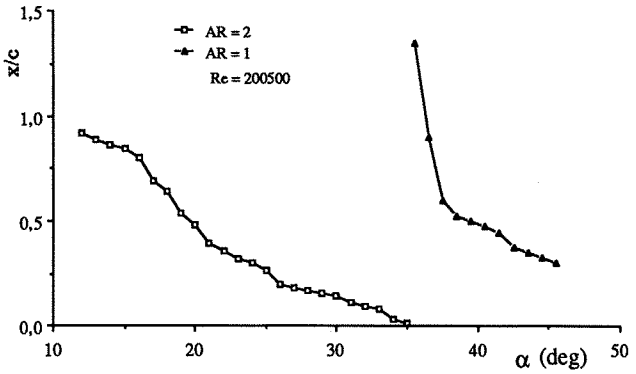

Figure 8. Breakdown locations vs. angle of attack in steady flow

wing-fixed x-coordinate of the burst point positions normalized to the root chord length of the wing vs. the angle of incidence. Each position is obtained from video frames using the digital image processing unit.

Increasing the angle of attack results in a displacement of the vortex burst points upstream towards the apex of the wing. At an angle of attack of about 10 degrees the vortex breakdown reach the trailing edge of the AR=2 wing in symmetrical flow. When the angle of attack is increased, the burst points move upstream progressively up to 20 degrees. A further increase of angle of attack shifts the burst points to the wing apex with a decreasing rate of displacement.

The delta wing with AR=1 shows a different behaviour. Below 35 degrees the vortex burst points are located downstream of the trailing edge. Increasing the angle of attack to about 37 degrees results in an abrupt movement upstream to a position of half the root chord of the wing. Slow motion video records show strong asymmetric locations of the burst points, even in symmetric flow generated by strong vortex interactions and, of course, model asymmetries. A further increase of angle of attack again shifts the burst points to the apex with a decreasing rate of displacement.

Unsteady Flow

Changing the angle of attack of the AR=2 delta wing by a plunging motion results in an approximately harmonic motion of the vortex burst points above the wing. This motion has hys-

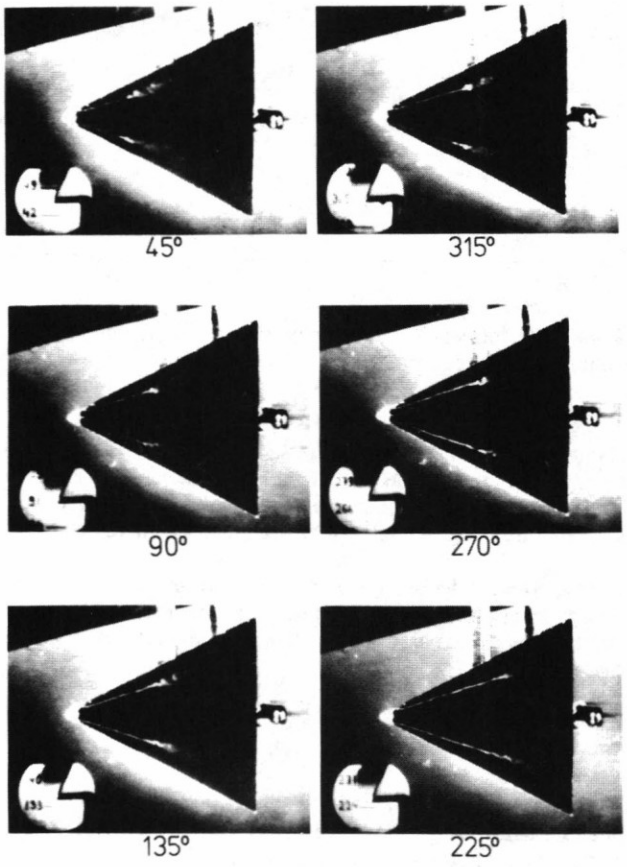

Figure 9. Flow pictures illustrating the hysteresis effect on breakdown positions in plunging motions

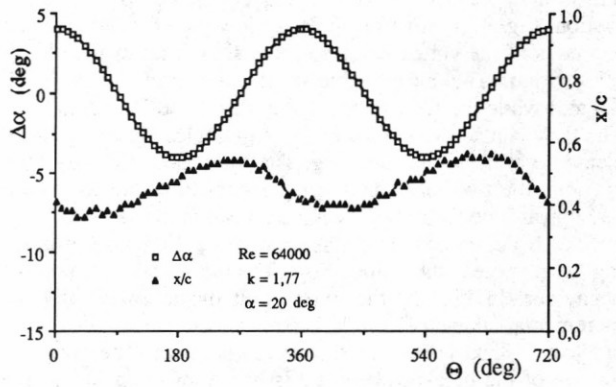

Figure 10. Phase lag between angle of attack and breakdown position

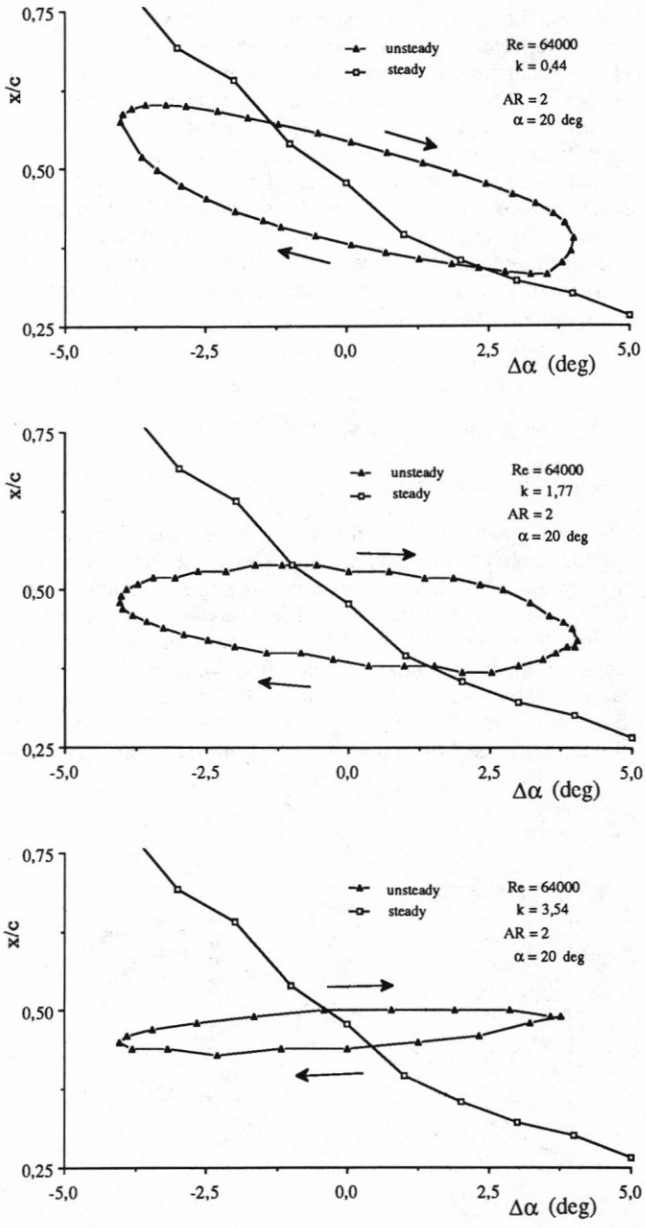

Figure 11. Hysteresis loops of breakdown displacements at three reduced frequencies

teresis and considerable phase lag compared to the model motion. Fig. 9 gives an example of flow pictures showing the locations of the vortex burst points at six phases of the plunging motion. The mean value of the angle of attack is 20 degrees while the reduced frequency of the motion (k) is 1.77. The flow is made visible by hydrogen bubbles generated by an electrode at the tip of the wing. The hysteresis is clearly seen between the two different burst point locations at downward and upward motions of the wing, recorded at the same angle of attack. Evaluation of these video frames by the image processing unit gives the time histories of vortex breakdown behaviour. In Fig. 10 the burst point displacement and the incremental angle of attack is shown vs. the angle of the crankshaft disk, which corresponds to the time. The upstream motion of the breakdown points is nearly twice as fast as the downstream motion. This causes a considerable phase lag between plunging motion and flow conditions.

Fig. 11 show the hysteresis loops of the burst point displacement vs. the incremental angle of attack for various frequencies. One frequency corresponds to the case of Fig. 10. There is a distinct hysteresis loop also at the lowest frequency as shown in Fig. 11. By increasing the frequency at the same incremental angle of attack (kept constant by reducing the amplitude of motion) the hysteresis loop first gets broader compared to the quasi-steady case. Then, the inclination of the mean axis to the steady curve becomes larger, which corresponds to an increase of phase lag in the time domain. Phase lags of more than 180 degrees can be found. A further increase of frequency results in a considerable reduction in the range of burst point displacement.

V. Wind-tunnel Results

Steady Symmetrical Flow

The breakdown behaviour discussed above has a strong impact on the aerodynamic coefficients. The lift coefficient in the aerodynamic coordinate domain vs. the angle of attack is given in Fig 12 for both delta wings. The breakdown displacements of Fig. 8 are related to the lift curve characteristics. Up to an angle of attack of 10 degrees the lift curve of the AR=2 wing shows a non-linear increase, caused by vortex lift. When the burst points reach the trailing edge a gradual reduction of lift increase results. Maximum lift occurs at an angle of attack of about 37 degrees. At this value the burst points are located close to the apex of the delta wing. A further increase of the angle of attack effects an abrupt decrease of lift followed by a smoother decrease at angles of attack greater than 42 degrees.

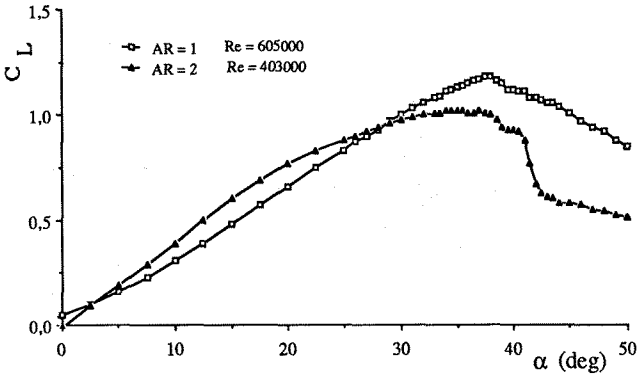

Figure 12. Steady lift coefficients of delta wings with aspect ratios AR=1 und AR=2

For the AR=1 delta wing, the maximum lift is correlated to the above mentioned abrupt displacement of the vortex burst points. This results in a sudden change of sign of the lift curve slope.

Steady Unsymmetrical Flow

For the AR=1 delta wing the influence of a sideslip on the lift, pitching and rolling moments is given in Fig. 13. An increase of the angle of sideslip reduces the vortex lift and diminishes the maximum lift. Also, instead of a marked peak in the lift curve, there is now only a flat plateau. It should be mentioned

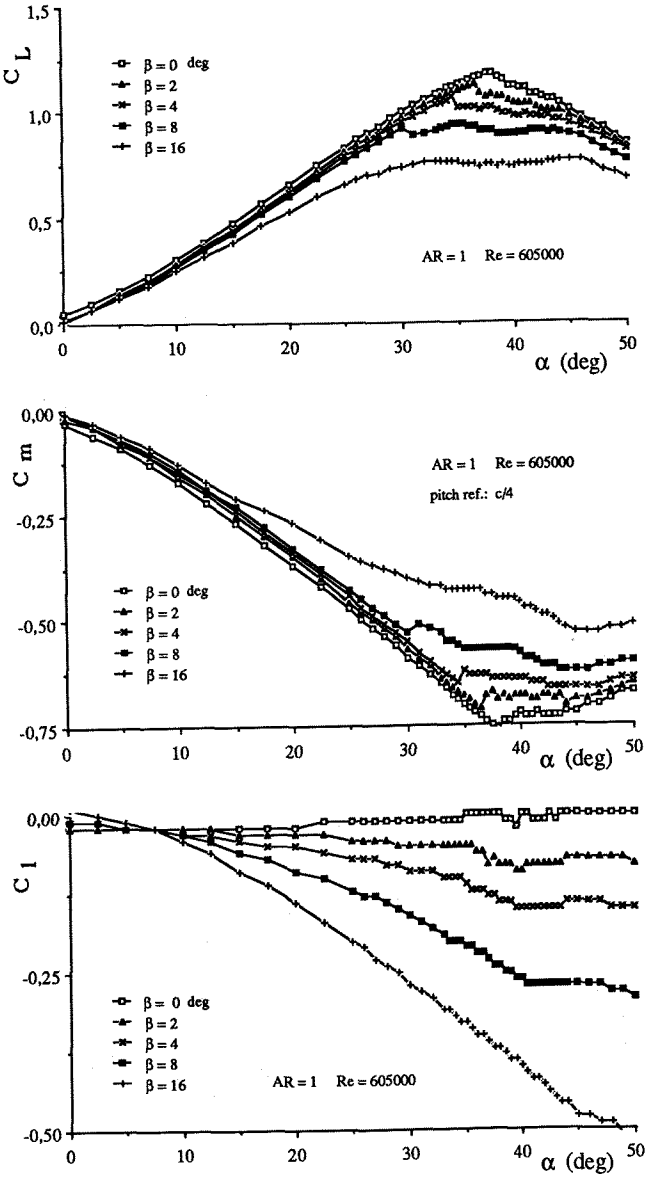

Figure 13. Influence of sideslip on steady lift, pitching and rolling moment coefficients

that the largest angle of sideslip (16 degrees) is larger than the semi apex angle of the AR=1 delta wing. Because the pitching moment is determined by lift and drag characteristics, the influence of the plateau of lift can only approximately be found. Positive angles of sideslip effect large negative rolling moments. These are caused by the large asymmetry in position and strength of the leading edge vortices. The breakdown influences the slope of the rolling moment vs. angle of attack in a similar way to that found in the pitching moment curves. In both cases a larger sideslip shifts the angle of attack where the curve slope changes sign to higher values. This is because the breakdown of the leeward vortex above the wing occurs at a higher angle of attack.

Wind-tunnel Results for Sinusoidal Gust Disturbance

In the following, the influence of sinusoidal gusts on lift and pitching moment is discussed. The aerodynamic coefficients show similar hysteresis loops to that found in the investigation of vortex breakdown in the water-tunnel.

Fig. 14 shows the lift coefficient of the AR=2 delta wing, which is disturbed by gusts for three values of reduced frequency. The mean angle of attack of the fixed delta wing was 20 degrees and the gust generator produced a nearly sinusoidal disturbances with an incremental incidence of 4 degrees.

Even at the lowest frequency, the mean value of the unsteady lift is somewhat lower than the steady value. This may be because the nozzle of the wind-tunnel is blocked a bit by the gust generator. The correction of the energy loss in the wind-tunnel nozzle, determined by the ratio of the differential pressure of the nozzle to the total pressure in the test section, has been done with the same factor for steady and unsteady measurements. Further tests have shown that this factor differs by about 3% between steady and unsteady flow conditions. This brings the unsteady mean value closer to the steady case. Another reason is that the unsteady mass forces have to be neglected (assuming that they are small because of the low bending of the strain gage balance).

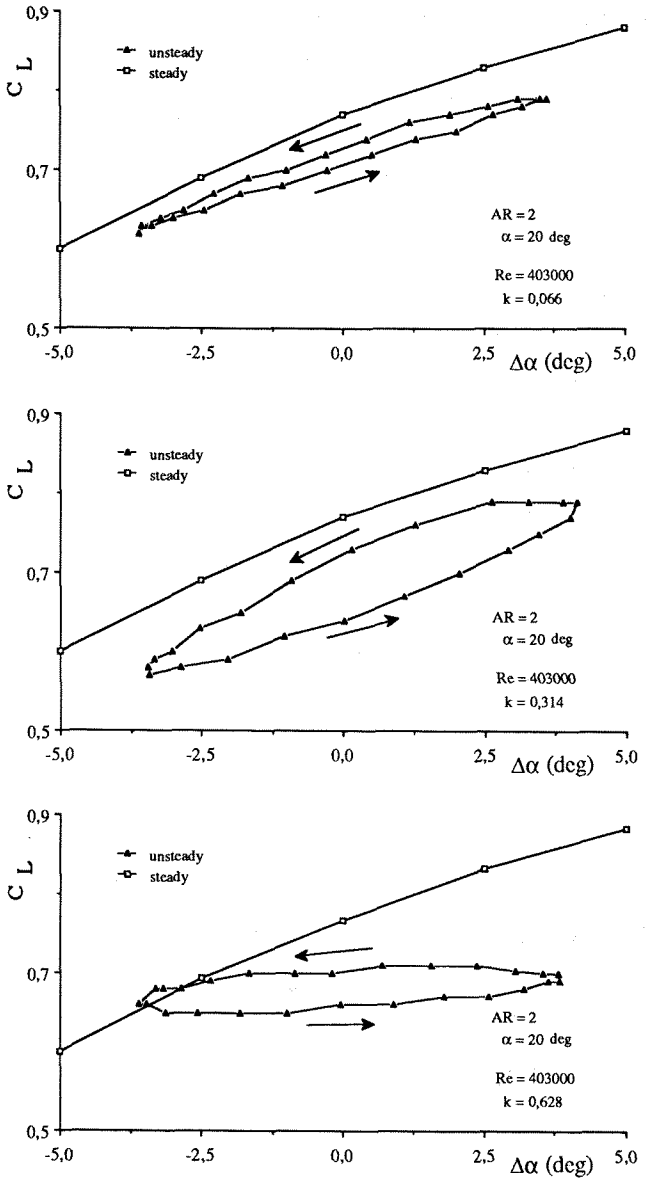

Figure 14. Hysteresis loops of unsteady lift coefficients (AR=2)

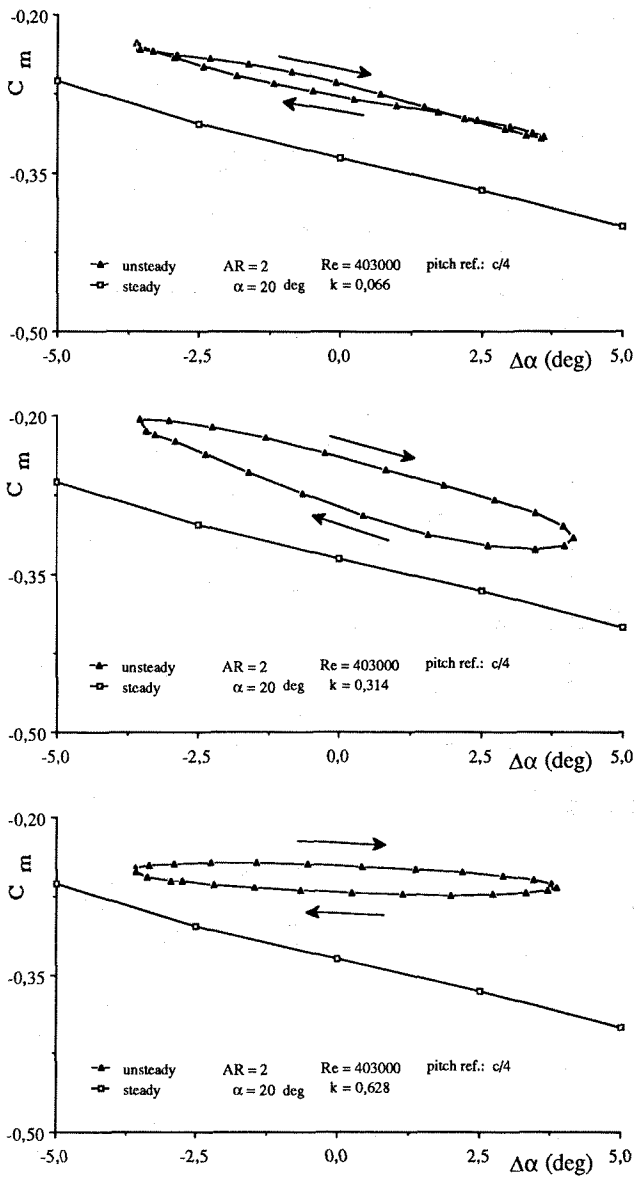

Figure 15. Hysteresis loops of unsteady pitching moment coefficients (AR=2)

An increase of the reduced frequency results in a widening of the hysteresis loop. This behaviour corresponds to the vortex burst point displacements shown in Fig 11. At lower frequencies the mean axis of the hysteresis loop is nearly parallel to the slope of the steady lift curve. Increasing the gust frequency at first increases the width of the hysteresis loop. Afterwards, the width decreases and the slope of the hysteresis axis is reduced. This effect coincides with a reduction of the range of breakdown displacement, as shown by flow visualization in the water-tunnel. The pitching moment curves, shown in Fig. 15, closely follow the lift curve loops. The high degree of similarity in the hysteresis loops of the water-tunnel and wind-tunnel results indicates that the time dependent behaviour of the forces and moments is strongly influenced by the vortex breakdown behaviour. The increasing phase lags, corresponding to the decreasing slope of the hysteresis axis, have a strong effect on the flight dynamic characteristics, even if the amplitudes of incremental lift and pitching moment decrease at higher reduced frequencies. At an angle of attack of 20 degrees, no bursting of the leading edge vortices was observed in water-tunnel tests of the delta wing with AR=1. Therefore, it is to be expected that the impact of the vortex lift on forces and moments is stronger than for the wing of AR=2. Fig. 16 confirms this insofar as larger increments in pitching moment are observed also at higher frequencies. The frequency at which the flow field cannot follow a change in angle of attack, indicated by a decrease of the incremental pitching moment, is shifted to higher reduced frequencies.

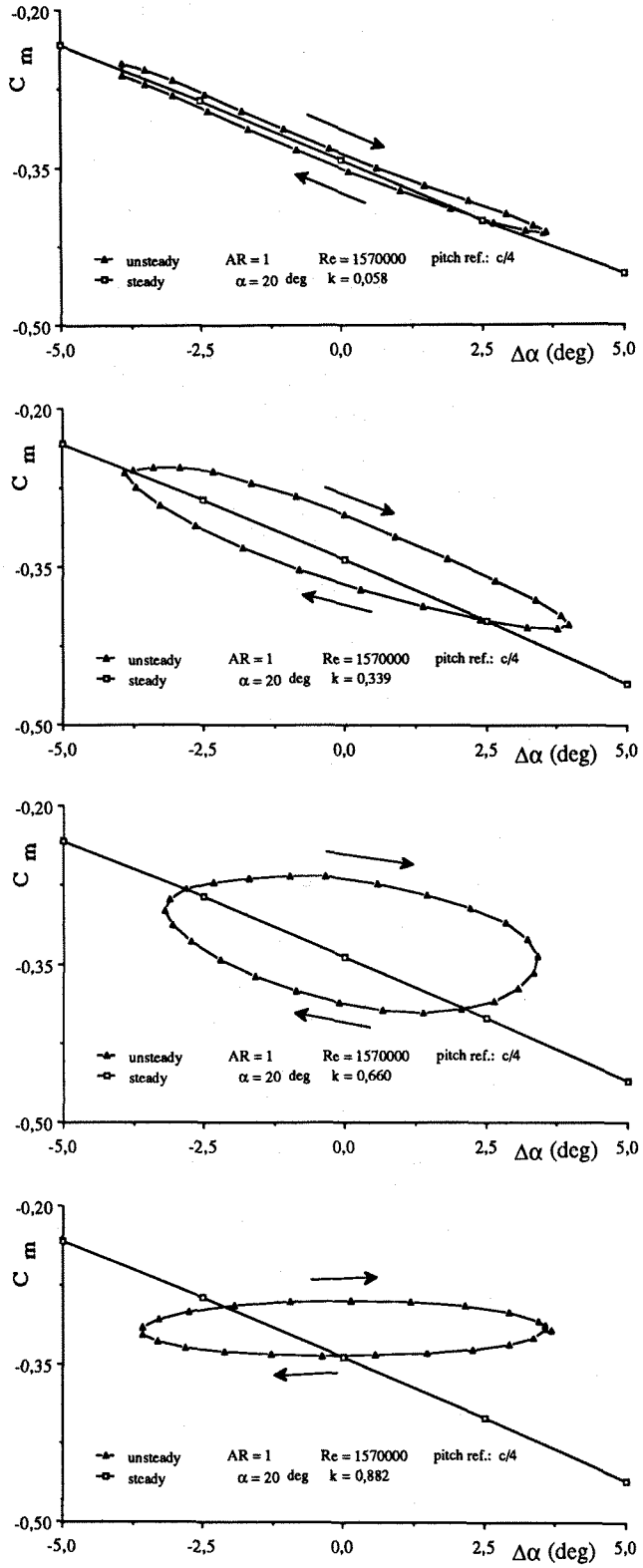

Figure 16. Hysteresis loops of unsteady pitching moment coefficient (AR=1)

Fig. 17 shows the increment of pitching moment coefficient vs. the reduced frequency with a variation of the Reynolds number for the delta wing of AR=1. As is well-known from results in steady flow, the influence of the Reynolds number is also small for the unsteady case. All data can be approximated

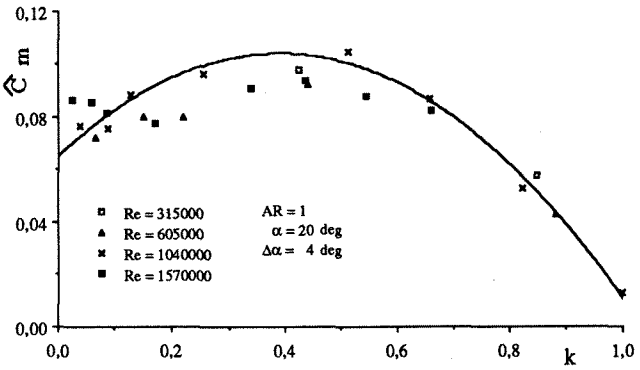

Figure 17. Amplitudes of the pitching moment coefficient as a function of reduced frequency

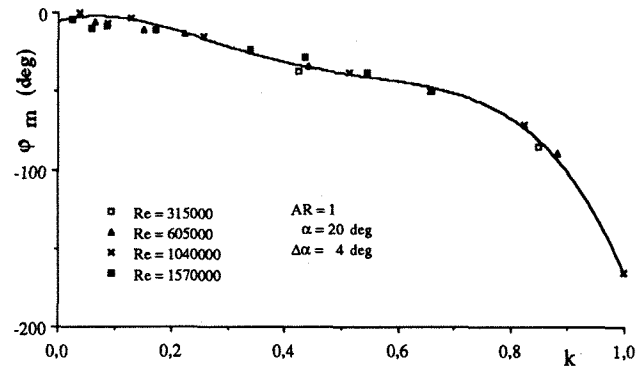

Figure 18: Phase lag of the pitching moment coefficient as a function of reduced frequency

by one curve. This diagram might imply that, except for the highest frequencies, there is only a small influence of reduced frequency on the increments. However, the hysteresis loops of Fig. 16 show that two different mechanisms determine the behaviour at lower and higher frequencies. In the range of quasi-steady flow, the variation of the pitching moment is characterized by the slope of the steady curve. At higher frequencies, a widening of the hysteresis loops occur. In this case the amplitudes of pitching moment and lift variations are given by the vertical widths of these loops.

For investigations of the flight dynamic characteristics, it is necessary to consider the phase lags between gust disturbance and aerodynamic forces. The time function of the gust is measured by the split-film probe, which gives the incremental angle of attack. This probe is located in the test section of the wind-tunnel at a position of half the wing root chord. This is also the position of the aerodynamic center of the delta wings.

For the AR=1 delta wing, the measured phase lags of pitching moment vs. reduced frequency are given in Fig. 18. Again, the influence of the Reynolds number on the phase lag is found to be negligible. At lower frequencies the behaviour of the phase lag is almost linear. The few data obtained at higher reduced frequencies suggest a progressive increase in phase lag. Thus, phase angles of up to 90 degrees can be observed.

All results discussed in this chapter concern the wings at 20 degrees mean angle of attack. For the AR=1 delta wing, the vortex burst points are located downstream of the trailing edge. As known from flow visualization, the vortex breakdown points reach the trailing edge at an incidence of about 36 degrees. The effect of vortex bursting is shown in Fig. 19 where the phase lag of pitching moment vs. mean angle of attack is plotted for different reduced frequencies. Up to the angle of attack where the wing is affected by the vortex breakdown over the wing, the phase lag curve is almost linear, with a well-ordered dependence upon the reduced frequency. At higher angles of attack, vortex breakdown above the wing leads to significant time lags of more than 180 degrees.

Wind-tunnel Results for Plunging Wings

Finally, a few results regarding the behaviour of a plunging delta wing will be discussed. All test have been done using the AR=1 delta wing with heave amplitudes of 4 degrees. The experiments were done in two steps. First, for obtaining the mass forces, measurements were performed by plunging the delta wing with no wind-tunnel blowing. Afterwards, combined mass and aerodynamic forces were measured. The evaluation of these tests requires a subtraction of the two data files. Fig. 20 presents first results obtained by this data reduction. The phase lag at higher values of mean incidence is quite similar to the results obtained in the gust investigations. At lower incidence, however, there is a considerable scattering of the data and the phase lag is smaller than that obtained in the gust case. Additional investigations should be performed to reduce the scattering. Furthermore, these results have shown the necessity of improving the test facilities and data reduction software. Preceding tests of the normal frequencies of the strain gage balance revealed a lowest normal frequency in lift force direction which was only four times larger than the maximum plunging frequency. This ratio is quite small. As a result, resonance effects could be a reason for the observed irregular behaviour of the phase lags. A new balance with larger stiffness is being built.

VI. Semi Empirical Estimation of Flight Dynamics

The Data Base

As seen in the foregoing part, vortex breakdown on delta wings results in quite different aerodynamic behaviour in steady and unsteady flow conditions. It would be of interest to see how these unsteady phenomena affect the motion of airplanes having delta wing configurations.

In the present section a method is proposed for converting the experimental data into a mathematical form suitable for incorporation in the equations of motion of aircraft. In the next section, results are shown for a representative configuration, to explore the effect of vortex breakdown on longitudinal aircraft motion.

It is evident from the experimental results that the vortex breakdown causes unsteadiness in aerodynamic forces. The major differences between steady and unsteady cases are that the amplitude is frequency dependent and phase lags occur in aerodynamic forces and moments.

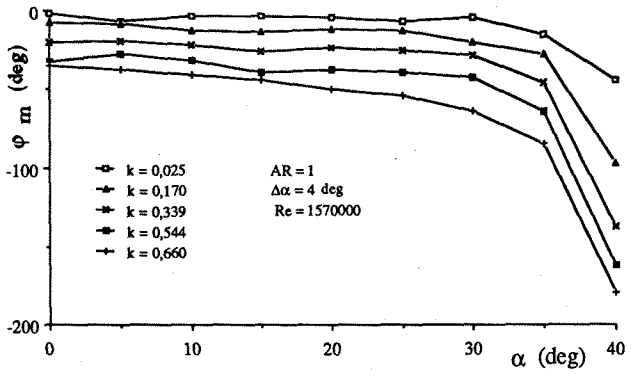

Figure 19. Phase lag of pitching moment coefficient vs. mean angle of attack (AR=1)

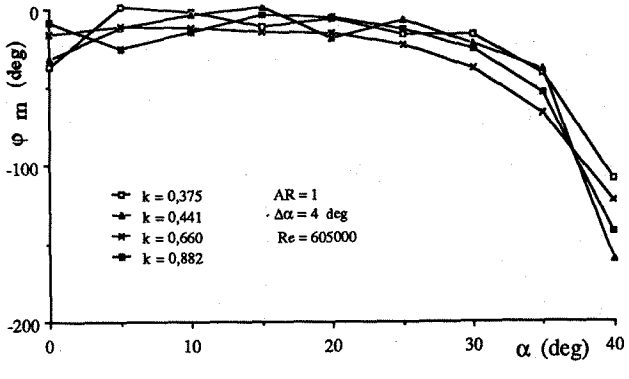

Figure 20. Phase lag of unsteady pitching moment coefficient for a plunging delta wing (AR=1)

Because the wind-tunnel results of the plunging delta wing are not sufficiently reliable at present, the influence of vortex breakdown on the forces and moments are obtained by a quasi-steady approximation correlating unsteady water-tunnel and steady wind-tunnel results, obtained for a delta wing of AR=2. The quasi-steady approach relates the vortex burst point positions evaluated under unsteady flow conditions at an angle of attack of $\alpha(1)$ to the angle of attack $\alpha(2)$, which provides the same burst point position in steady flow. Fig. 21 gives an example for the case of Fig. 11. Then, lift and pitching moment are obtained from the steady wind-tunnel results in the following manner. Fig. 22 shows the measured steady lift curve (curve a), where the breakdown effects lead to a decreasing slope. In addition, an estimation of the lift curve including full vortex lift (without breakdown) is included in the diagram (curve b). The loss in lift due to breakdown is the difference between curve b and curve a. This value is taken at $\alpha(2)$ and subtracted from the lift taken from curve b at $\alpha(1)$.

In this way, for all points of the breakdown hysteresis loop, lift and pitching moment can be obtained as a function of time, including effects of the phase lags. These data have been used for the following preliminary study of flight dynamic behaviour.

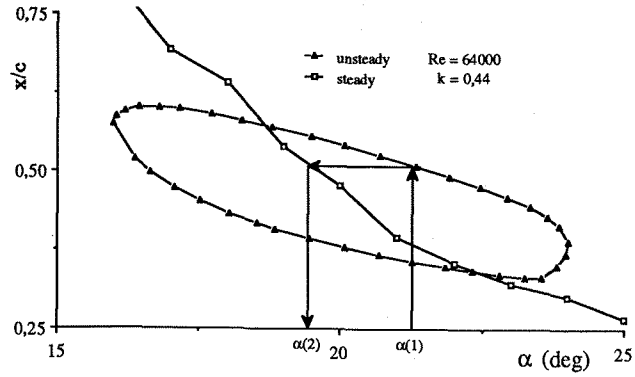

Figure 21. Correlation between steady and unsteady breakdown locations

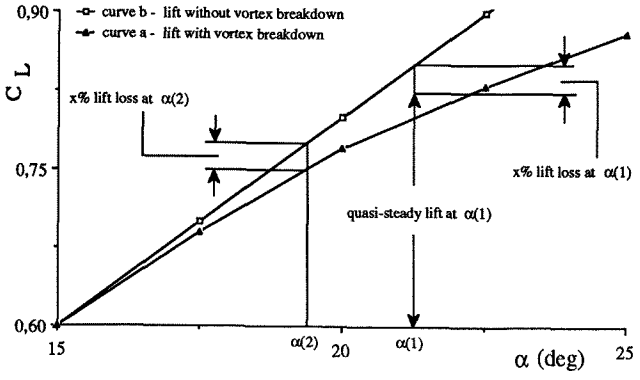

Figure 22. Quasi-steady estimation of breakdown influence on lift

The Basic Approach

For treating unsteady dynamical problems, a great deal of work has been done in the past. Classical research on unsteady aerodynamics, such as by Theodorsen, Kuessner, Sears and Jones et al., was mainly aimed at the flutter problem. This was based on the method of Aerodynamic Influence Coefficients (AIC), where the airplane response is computed for simple harmonic motion at discrete values of reduced frequency. Modern control analysis calls for the representation of the aerodynamic forces in the entire Laplace domain, so that the state equation in matrix form can be formulated for linear stability analysis. For this purpose, the aerodynamic transfer function (ATF) has to be approximated by rational functions of the Laplace operator, s.

Following Dowell's suggestion[15], the following expression defining the basic structure of the ATF is chosen:

$$ATF(\bar{s}) = \sum_{i=1}^{m} \frac{a_i \bar{s}}{\bar{s} + b_i} \qquad (1)$$

where $\bar{s}=sc/2U$ is the non-dimensional Laplace operator. To determine the system order m and the coefficients a and b, a parameter identification procedure has been developed by using a direct search optimization algorithm[16]. A computer program has been developed which automatically determines a and b for a specified value of m. The selection of m is based on the requirements of accuracy and the minimum-state. To approximate the measurements, the least-square error for both amplitude and phase angle is simultaneously achieved by minimizing the cost function:

$$J = (1/N) \sum_{i=1}^{N} \left\{ \left[K_{ai} \Delta A(\omega_i) \right]^2 + \left[K_{fi} \Delta \varphi(\omega_i) \right]^2 \right\} \qquad (2)$$

where $\Delta A(\omega_i)$ and $\Delta\varphi(\omega_i)$ are the errors of amplitude and phase angle at each selected frequency. K_{ai} and K_{fi} are weighting factors for amplitude and phase angle, respectively. In order to achieve better correspondence with the measured data, it seemed suitable to interpolate the original data set at 20 equidistant frequencies.

Fig. 23 shows an example of the approximating process for the delta wing of AR=2. The identified parameters are m=3, a_1 =0.9822, a_2 =0.3170, a_3 =-2.4644, b_1 =0, b_2 =2.8869, b_3=4.3575. This approximation provides a quite good agreement with the measured values of phase lag and amplitude ratio.

Simulation of the Dynamic Response

Equation (1) is the basis for accounting for unsteady aerodynamic effects due to vortex breakdown. These effects are inserted into the linearized, small perturbation equations of motion for a rigid airplane. The assumed longitudinal equations of motion have the form:

$$\begin{aligned}
\Delta \dot{U} &= -g\Delta\gamma + (\rho U^2 S/2m)\Delta C_x \\
\Delta \dot{\alpha} &= \Delta q + (\rho U S/2m)\Delta C_z \\
\Delta \dot{q} &= (\rho U^2 S \bar{c}/2I_y)\Delta C_m \\
\Delta \dot{\theta} &= \Delta q
\end{aligned} \qquad (3)$$

Equation (3) can be rewritten in matrix form

$$\dot{\underline{X}}_s = \underline{A}_s \underline{X}_s + \underline{B}_s \underline{U} \qquad (4)$$

The unsteady effects are inserted into the equations of motion through C_z and C_m according to equation (1). Due to the fact that the aerodynamic coefficients depend upon the aircraft motion, i. e. $\underline{X}_a = F(\underline{X}_s)$, the ATF can be converted into a matrix equation in the time domain

$$\dot{\underline{X}}_a = \underline{A}_a \underline{X}_a + \underline{B}_a \underline{X}_s \qquad (5)$$

The subscripts s and a in (4) and (5) denote state variables and aerodynamic coefficients, respectively. By combining Eq. (4) with (5) the equations of motion can be written as

$$\dot{\underline{X}} = \underline{A}\,\underline{X} + \underline{B}\,\underline{U} \qquad (6)$$

where

$$\underline{X} = (\underline{X}_s\ \underline{X}_a)^T$$

The output equation is generally given in the form

$$\underline{Y} = \underline{C}\,\underline{X}$$

Numerical Example and Results

For testing the influence of the unsteady effects, a hypothetical supersonic transport aircraft with a delta wing of AR=2 has been chosen. The main parameters of the airplane are given as

total weight: m= 160 t
moment of inertia: I = 3,200,000 kgm^2
wing area: S = 780 m^2
mean aerodynamic chord: c = 38 m
span: b = 57 m

The aerodynamic derivatives for pitch rate, C_{mq} and C_{Lq}, were approximately evaluated. For simplicity, the contribution of the horizontal tail to unsteady aerodynamic loads was neglected.

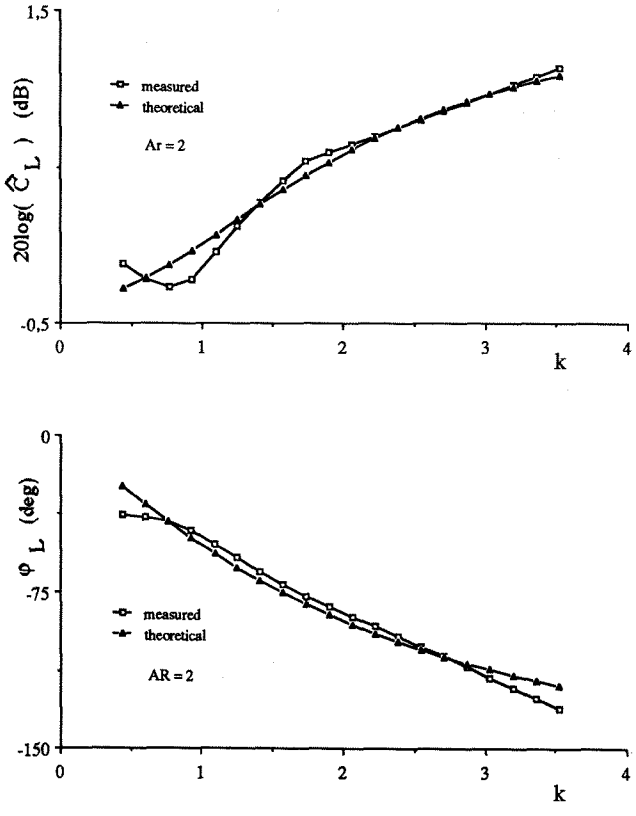

Figure 23 Approximations of lift amplitude and phase lag curves plotted against reduced frequency

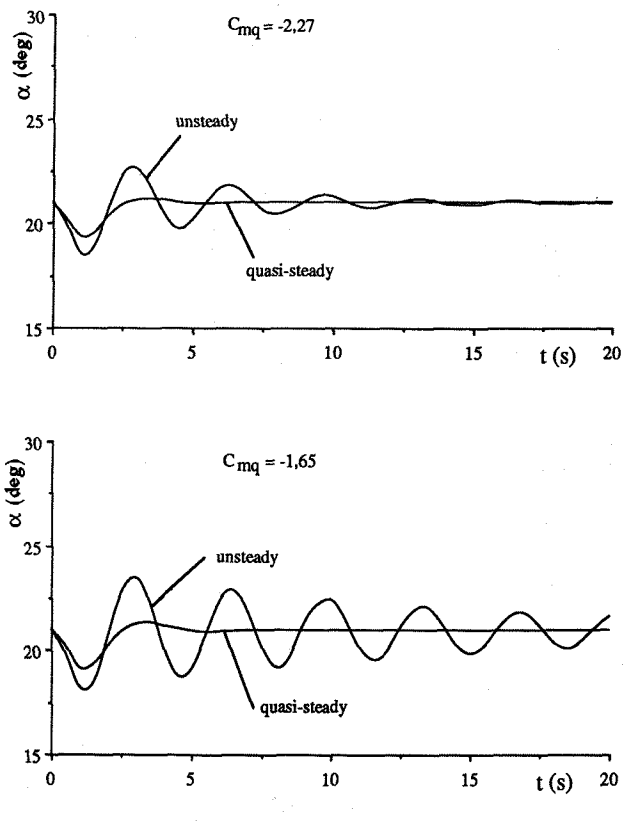

Figure 24. Time history of angle of attack following a (1 - cos) elevator disturbance for quasisteady and unsteady aerodynamics

The undisturbed flight condition is at sea-level at a speed of 83m/s. The trimmed angle of attack is 20 degrees. A disturbance is applied to the dynamic system by an elevator deflection in (1-cos) form with a 10 degrees amplitude and a period of one second.

The simulation results, comparing quasi-steady and unsteady cases, are presented in Fig. 24 a and, in Fig. 24 b, there is a case with 25% reduction in pitch damping. It is obvious that the inclusion of vortex breakdown features in the aerodynamic representation has a pronounced effect on angle of attack response. Only a small effect on the phugoid mode is to be expected.

It should be mentioned that the results presented here are only qualitatively correct. The aerodynamic transfer function, identified here by a few measured data in certain frequency regions has to be generalized to the whole s-plane or, in other words to arbitrary motion. However, the experimental data are available only at a few discrete frequencies. This may degrade the accuracy of the numerical results. Nevertheless, the simulated results indicate pronounced effects of unsteady vortex breakdown phenomenon on airplane motion.
Further research work should be done with a more sufficient experimental data base. The analysis method should be modified to account for a more sophisticated dynamic system model, which may include an automatic control system and some structural modes.

VII. Concluding Remarks

1) Two delta wings with aspect ratios of 1 and 2 have been studied under unsteady conditions, generated by a gust-generator and by plunging movements in a water-tunnel and a wind-tunnel.

2) At higher angles of attack, the breakdown of the leading edge vortices lead to hysteresis loops and time lags in aerodynamic forces and moments. These can be directly correlated with the unsteady displacement of the breakdown points above the delta wings.

3) Influences on the flight dynamic characteristics of a delta wing configuration have been demonstrated where, in particular, the damping of the short period mode is reduced.

4) Further work has to be done to refine the experimental and theoretical tools. An extension to study the lateral dynamic behaviour should be done.

Acknowledgments

The authors wish to thank the Deutsche Forschungsgemeinschaft (DFG) for the financial support of this research.

References

1. Herbst, W. B., "Future Fighter Technologies", Journal of Aircraft, Vol. 17, No. 8, August 1980, pp. 561.

2. Kraus, W., "Delta Canard Configuration at High Angle of Attack", Z. Flugwiss. Weltraumforsch. 7 (1983), Heft 1, pp. 41.

3. Earnshaw, P. B.; Lawford, J. A., "Low-Speed Wind-Tunnel Experiments on a Series of Sharp-Edged Delta Wings", Aeronautical Research Council, Reports and Memoranda No. 3424, March 1964.

4. Lambourne, N. C.; Bryer, D. W.; Maybrey, J. F. M., "The Behaviour of Leading Edge Vortices over a Delta Wing Following a Sudden Change of Incidence", Aeronautical Research Council, Reports and Memoranda No. 3645, March 1969.

5. Parker, A. G., "Measurements on a Delta Wing in Unsteady Flow", Journal of Aircraft, Vol. 14, No. 6, June 1977, pp. 547.

6. Carcaillet, R.; Manie, F.; Pagan, D.; Solignac, J. L., "Leading Edge Vortex Flow Over A 75 Degree-Swept Delta Wing - Experimental and Computational Results", 15. ICAS-Kongreß, London 7. - 12. September 1986, ICAS-Proceedings 1986, Vol. 1, pp. 589.

7. Gad-El-Hak, M. ; Ho, C.-M., "The Pitching Delta Wing", AIAA-Journal, Vol. 23, No. 11, November 1985, pp. 1660.

8. Becker, J.; Gravelle, A., "Some Results of Experimental and Analytical Buffeting Investigations on a Delta Wing", ONERA-TP-1985-59.

9. Atta, R.; Rockwell, D., "Hysteresis of Vortex Development and Breakdown on an Oscillating Delta Wing", AIAA-Journal, Vol. 25, No. 11, November 1987, pp. 1512.

10. Orlik-Rueckemann, K. J.; Hanff, E. S., "Dynamic Stability Parameters at High Angles of Attack", 12. ICAS-Kongress, München 12. - 17. October 1980, ICAS-Proceedings 1980, pp. 265.

11. Staufenbiel, R.; Steckemetz, B., "Der Einfluss periodischer Anstellwinkeländerungen auf das Aufplatzverhalten von Deltaflügel-Vorderkantenwirbeln",5.DGLR-Fach-Symposium "Strömungen mit Ablösung", München, 9./10. Oktober 1986.

12. Staufenbiel, R.; Steckemetz, B., "Instationäre Vorgänge an Deltaflügeln mit teilweise aufgeplatzten Wirbelbereichen", in: Mitteilung aus dem Institut für Luft- und Raumfahrt der RWTH Aachen, Heft 3, S. 117, Aachen, Oktober 1987.

13. Steckemetz, B.; Staufenbiel, R., "Untersuchung des Wirbelsystems eines Deltaflügels unter Böenbeaufschlagung im Unterschall-Windkanal", Lecture, Workshop der Arbeitsgruppe "Experimentelle Methodik" im DFG-Schwerpunkt "Physik abgelöster Strömungen", Berlin (West), 3./4. März 1987.

14. Steckemetz, B.; Staufenbiel, R., "Druckverteilungsmessungen an einem scharfkantigen Deltaflügel bei harmonischer Anstellwinkeländerung", Lecture, 3. Workshop der Arbeitsgemeinschaft "Strömungen mit Ablösung", Göttingen, 10./11. November 1987.

15. Jacob, H. G., "Rechnergestützte Optimierung von Statischen und Dynamischen Systemen", Institut für Flugführung der TU Braunschweig, Februar 1981.

16. Dowell, E. H., "A Simple Method for Converting Frequency- Domain Aerodynamics to the Time Domain", NASA TM-81838, 1980.